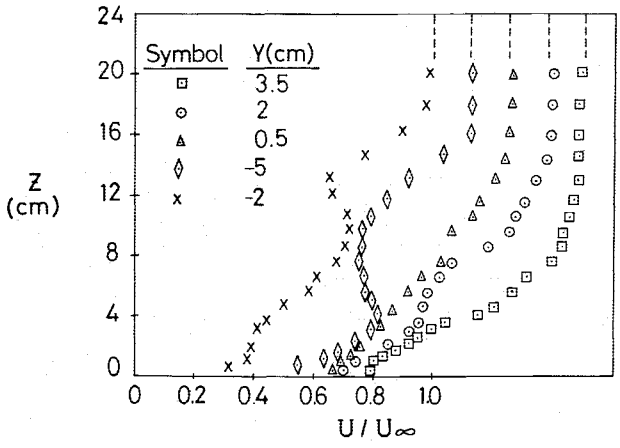

Fig. 4 Vertical variation of normalized stream-wise velocity U/U_∞ for $Y = 3.5$, 2, 0.5, -2, and -5 cm at $X = 29.5$ cm.

projection of the wing on the plane of the figure. The saddle and nodal-type singular points in the streamline pattern are denoted by letters S and N, respectively. The horizontal line elements attached to the Y = constant lines show both the magnitude and direction of the span-wise velocity (V) measured at this particular X location. The velocity data support the validity of the hypothesized streamline pattern. The tip vortex is located at a higher Z location than the tornado vortex. The tip and tornado vortices are deflected in the negative Y direction as they move downstream. This is probably due to the inviscid turning of the freestream by the wing in the negative Y direction. The large negative V velocities in the $Y > 0$ region away from the flat plate also indicate such an inviscid flow deflection. The span-wise velocities given in Fig. 3 confirm that the $Y > 0$ leg of the horseshoe vortex is larger and stronger than the $Y < 0$ leg.

Figure 4 gives the vertical variation of the normalized stream-wise velocity U/U_∞ for various Y locations at $X = 29.5$ cm. The origin of the plot is displaced to the right by 0.125 for each of the Y stations. The location of $U/U_\infty = 1$ for each profile is denoted by dotted lines. Figure 4 shows that the normalized stream-wise velocity U/U_∞ increases monotonically with increasing Z in the $Y > 0$ region, whereas the stream-wise velocity profiles in the $Y < 0$ region exhibit S-shaped variations in the Z direction. It appears that the tip vortex and the tornado vortex that are both located in the $Y < 0$ region are responsible for the S-shaped profiles. Trentacosta and Sforza[4] report irregularities in stream-wise velocity profiles around the potential cores of three-dimensional jets. They suggest that the irregularities are generated by the induced velocities of a decaying vortex ring surrounding the jet. It may be argued that as the longitudinal tip and tornado vortices are deflected in the negative Y direction, they become capable of inducing a stream-wise velocity component in the surrounding fluid and, thus, generate the S-shaped profiles. A vortical flow structure similar to the Karman vortex street can also be responsible for the generation of S-shaped profiles. Morrisette and Bushnell[2] also observe irregular-shaped stream-wise velocity profiles in the wake of a wedge at zero angle of attack. They report that longitudinal vortices, which originate from the vicinity of the wake neck, are the cause of large deficits in the streamwise velocity. Morrisette and Bushnell[2] hypothesize that the concave curvature of the shear layer approaching the wake neck leads to the generation of Taylor-Gortler vortices. Further experimental work is needed to check the existence of Taylor-Gortler-type vortices in the flow of the present study. Conversely, one may hypothesize that the vortices observed in Ref. 2 are a pair of tornado vortices that are fed by the flow separated from both two sides of the wedge. Tani et al.[5] observe two counter-rotating tornado vortices behind a cylinder mounted on a plate. Any evidence of a second tornado vortex could not be observed in the present study. This was probably due to the attached flow conditions on the windward side of the wing where flow separation from the trailing edge did not lead to a sufficiently large reversed-flow region.

References

[1]Nakayama, A. and Rahai, H. R., "Measurements of Turbulent Flow Behind a Flat Plate Mounted Normal to the Wall," *AIAA Journal*, Vol. 22, Dec. 1984, pp. 1817–1819.

[2]Morrisette, E. L. and Bushnell, D. M., "Evidence of Imbedded Vortices in a Three-Dimensional Shear Flow," *AIAA Journal*, Vol. 19, March 1981, pp. 400–402.

[3]Özcan, O. and Ölçmen, M. S., "Measurements of Turbulent Flow Behind a Wing-Body Junction," *Proceedings of the Sixth Symposium on Turbulent Shear Flows*, Toulouse, France, Sept. 1987.

[4]Trentacosa, N. and Sforza, P., "Further Experimental Results for Three-Dimensional Free Jets," *AIAA Journal*, Vol. 5, May 1967, pp. 885–891.

[5]Tani, I., Komoda, H., Komatsu, Y., and Iuchi, M., "Boundary-Layer Transition by Isolated Roughness," Rept. No. 375, Aeronautical Research Inst., Univ. of Tokyo, Nov. 1962.

Turbulent Viscous Drag Reduction with Thin-Element Riblets

B. Lazos* and S. P. Wilkinson*
NASA Langley Research Center, Hampton, Virginia

Introduction

THE parametric studies by Walsh and Lindemann[1] of various riblet geometries established the symmetric V-groove riblet as a practical means for turbulent viscous drag reduction. In an effort to improve riblet performance, an experimental program was initiated to extend the riblet data base to additional, untested riblet geometries. One achievement of this program was the identification of the thin-element, rectangular geometry with a maximum drag reduction equal to the symmetric V-groove (8%) and drag reduction at larger riblet spacings.

The current geometry consists of very thin ribs extending perpendicularly from the wall and aligned in the streamwise direction. They form an array of streamwise channels in the near-wall region whose height and spacing may be varied independently without affecting the spanwise contour of the region between adjacent riblets. Independent height and spacing control is a particularly desirable feature for proper parametric study. This geometry was selected for direct drag study primarily because of turbulence intensity data obtained for similar models in a previous study,[2] which showed a significant impact of the thin-element design on the intensity level and distribution.

Model Construction and Apparatus

Thin-Element riblet model construction is illustrated in Fig. 1a. As shown, thin metal strips were clamped between spacers defining the channel height and width. The metal strips had sharp, square edges and were 0.002 in. thick (approximately 1–2 viscous wall lengths). A more practical model in terms of potential application with a similar geometry was also tested and consisted of adjacent trapezoidal elements formed in con-

Received April 9, 1987; revision received June 1, 1987.

*Aerospace Engineer, Viscous Flow Branch, High-Speed Aerodynamics Division. Member AIAA.

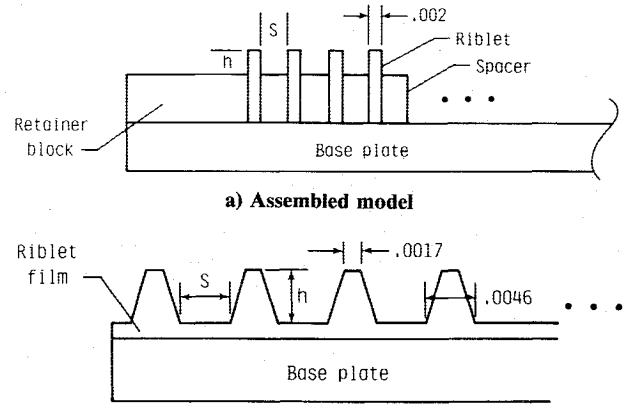

Fig. 1 Thin-element array models (cross-sectional and end view).

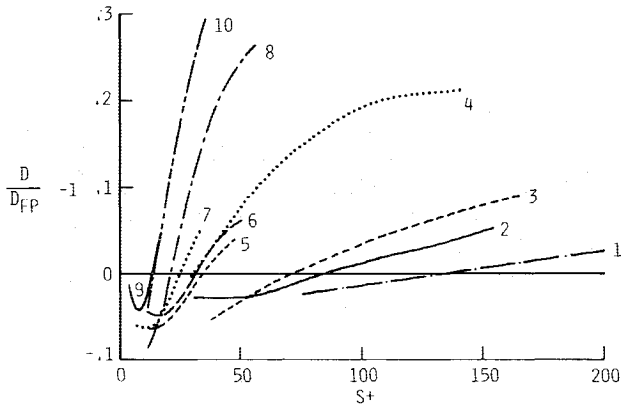

Fig. 2 Drag data for assembled and plastic film models.

Table 1 Model riblet dimensions

Model	Type	h(in.)	s(in.)	Aspect ratio (h/s)
	A	0.010	0.140	0.07
2	A	0.010	0.064	0.16
3	A	0.013	0.080	0.16
4	A	0.020	0.064	0.31
5	F	0.006	0.018	0.33
6	A	0.010	0.025	0.40
7	F	0.006	0.012	0.50
8	A	0.020	0.025	0.80
9	F	0.006	0.006	1.00
10	A	0.025	0.025	1.00

A = assembled model; F = plastic film model.

tinuous plastic film with an adhesive backing (Fig. 1b). Model dimensions are listed in Table 1 in order of increasing channel aspect ratio. Testing was conducted in the 7×11 in. Low-Speed Wind Tunnel at the NASA Langley Research Center[2] over a velocity range of 26–100 ft/s ($1000 < Re_\theta < 4000$) under nominally atmospheric conditions at a nearly zero steamwise pressure gradient. A portion of the tunnel test section floor was used as the test bed. There was no significant difference in drag between the models mounted with either peaks or valleys flush with the up- and downstream tunnel floors. Numerous flat-plate test runs were made with each model to establish the data trends and to guard against any anomalous data shifts. The experimentally determined reference flat-plate drag level for these tests is approximately given by the relation

$$D_{FP} = 8.23 \times 10^{-6}\, U_\infty^{1.82}$$

where English engineering units are used (D_{FP} in lbf and U_∞ in ft/s).

Experimental Results and Discussion

Figure 2 shows drag data for both assembled and plastic film models plotted with respect to riblet spacing in wall units, $s^+ = sU_\tau/\nu$, where s is the riblet spacing, U_τ the friction velocity, and ν the kinematic viscosity. The plastic film model data are seen to exhibit performance similar to the assembled models. Maximum drag reduction equal to 8% is achieved for model 8 at $s^+ = 12$ and $h^+ = 10$ ($h^+ = hU_\tau/\nu$, where h is the riblet height). This is similar to the best symmetric V-groove model,[1] which showed an 8% drag reduction at $s^+ = 15$ and $h^+ = 13$.

The data in Fig. 2 also show gradually diminishing drag reduction out to an s^+ value of 140. This is the highest reported s^+ value at which riblet drag reduction is still evident. In comparison, the V-groove riblets had drag reduction up to 50 wall units.[1] Drag reduction at high s^+ values is significant since it occurs in the range of observed low-speed streak spacings and may point to a mode of drag reduction associated with low-speed streak phenomena. Streamwise intensity profile measurements on a similar set of thin-element riblets having constant physical heights at a fixed stream velocity[2] showed a significant impact of riblet spacing on the longitudinal turbulence intensity distributions and levels. In particular, it was shown that an abrupt shift in the vertical location of the peak in the intensity profile above a valley occurs at between $s^+ = 50$ and 65. The peak location was relatively consistent on either side of the transition. This finding suggests an alternate mode of drag reduction that depends on whether the valleys are relatively quiescent ($s^+ < 50$) or more energetic ($s^+ > 65$).

This suggestion of more than one drag reduction mechanism tends to be contradicted, however, by the absence of any clearly abrupt behavior in the $s^+ = 50$–65 region of the drag data. It was also noted in Ref. 2 that the peak intensity level above a riblet valley was reduced by as much as 30% below the flat-plate levels ($s^+ = 50$). There is no evidence, however, that the integrated drag level is uniquely sensitive to even major changes in turbulence intensity. Cursory investigation of turbulence intensity levels above a valley on model 8 showed a significant maximum intensity reduction at stream velocities corresponding to increased as well as decreased drag. The only reasonable drag reduction mechanism appears to be the low-momentum, nearly Stokes-type flow afforded by properly sized riblet channels. It is conceivable that the large range of drag reduction associated with the thin-element riblets is due more to the fact that the rectangular, thin-element geometry maintains low-momentum (i.e., low-drag) regions of corner flow at any riblet spacing.

It was previously reported that a low-aspect-ratio symmetric V-groove (model 35 in Ref. 3, aspect ratio = 0.08) exhibited a uniform 4% drag reduction up to $s^+ = 200$. A retest of that same model failed to show any drag reduction, which supports the hypothesis of a single drag-reduction mechanism based on extended regions of quiescent near-wall flow alone. Figure 2 also shows consistent variation in the level and slope of the various curves as the riblet channel aspect ratio is varied. It is clear from Fig. 2 that, for drag ratios greater than zero, the drag is qualitatively roughly proportional to the riblet height and inversely proportional to the spacing. In this region, simple considerations of the separate influence of vertical and horizontal regions of the wetted-riblet area on the total drag under an assumed Reynolds number dependent mean velocity profile largely predicts this general behavior. Consistent trends in the drag reduction region are less evident. The maximum drag reduction level occurs only at high aspect ratios, with the best performance for this series of models occurring at an aspect ratio of 0.8 (model 8). This is consistent with the experimental findings of Walsh and Lindemann.[1] It is also consistent with the theoretical findings of Bechert et al.,[4] which show that protrusion height (a measure of the range of riblet influence normal to the wall) reaches a maximum at an aspect ratio of one.

Conclusions

Conclusions reached in the current study are:

1) Thin-element riblets are as effective in reducing drag as symmetric V-grooves, but exhibit a larger range of allowable spacings.

2) The thin-element geometry shows qualitatively predictable influence of independent variation of riblet height and spacing.

3) Evidence of more than one drag reduction mechanism for thin-element riblets is inconclusive.

References

[1]Walsh, M.J. and Lindemann, A.M., "Optimization and Application of Riblets for Turbulent Drag Reduction," AIAA Paper 84-0347, Jan. 1984.

[2]Wilkinson, S.P. and Lazos, B.S., "Direct Drag and Hot-Wire Measurements on Thin-Element Riblet Arrays," Paper presented at IUTAM Symposium on Turbulence Management and Relaminarization, Bangalore, India, Jan. 1987.

[3]Walsh, M.J., "Drag Characteristics of V-Groove and Transverse Curvature Riblets," *Progress in Astronautics and Aeronautics: Viscous Flow Drag Reduction*, Vol. 72, edited by G.R. Hough, AIAA, New York, 1980, pp. 168–184.

[4]Bechert, D.W., Bartenwerfer, M., and Hoppe, G., "Drag Reduction Mechanisms Derived from Shark Skin," Paper 86-1.8.3 presented at 15th Congress of the International Council of the Aeronautical Sciences, London, Sept. 1986.

Aerodynamic Interaction Tones of a Model Counter-Rotating Propeller

R. T. Nagel* and H. V. L. Patrick†
North Carolina State University, Raleigh, North Carolina

Introduction

IT has been well established that counter-rotating propellers (CRP's) are more efficient and exhibit significantly different radiated noise characteristics than single-rotation propellers (SRP's).[1] The difference in noise characteristics is primarily associated with interaction between the forward and aft propellers. The mechanism causing this aerodynamic interaction noise is not well understood, and numerous studies investigating this phenomenon have been initiated.

A series of radiated noise measurements using a Fairey Gannet AEW3 aircraft with CRP's have been reported[2] where the forward propeller rotated at a different rotational speed than the aft propeller. The investigation showed that the interaction noise could be identified in the noise frequency spectrum as discrete tones associated with the sums and differences of the forward and aft propeller blade-passing frequencies (BPF). These interaction tones were clearly different than the tones associated with single-rotation propellers and are similar to blade-vane interaction noise in ducted rotating machinery.

Presented as Paper 86-4.6.1 at the 15th ICAS Conference, London, England, Sept. 7-12, 1986; received July 20, 1987; revision received Sept. 22, 1987.

*Associate Professor, Department of Mechanical and Aerospace Engineering. Member AIAA.

†Visiting Instructor, Department of Mechanical and Aerospace Engineering. Senior Member AIAA.

A theory predicting interaction noise has been developed by Hanson[3] which requires the calculation of the unsteady forces for all radial positions of the blade. Unfortunately, the information required for this model is presently not available and would be very difficult to obtain.

From a fundamental point of view, the radiated noise generated by propellers is directly related to the flow through the blade disk. The flow over the blades generates forces (lift and drag) that in turn generates sound in the surrounding fluid medium. The flow between the forward and aft propellers of CRP contains both the response information of the upstream blades and the input information to the downstream blades. One may, therefore, hypothesize that the flowfield between the propellers would be directly related to the radiated aerodynamic interaction noise. It is likely that simple coherence, based on the flow fluctuations and interaction noise, will exist at any location where the flow signal contains information from both the forward and aft rotors.

By measuring the velocity field between the propellers and the radiated noise and then performing coherence analysis between the two different physical phenomena, correlation would be established if the given hypothesis is valid. Coherence $\gamma(f)$ is related to the autospectrum $G_v(f)$ of the fluctuating velocity in the flowfield, the autospectrum $G_p(f)$ of the radiated noise, and the cross-spectrum $G_{vp}(f)$ by the relationship

$$\gamma(f)=G_{vp}(f)/G_v(f)G_p(f) \tag{1}$$

where f is the frequency.

If $0<\gamma(f)<1$, one or more of the following possible explanations exists:[4] 1) random noise is present in the experiment, 2) the relationship between sound and velocity is not linear, and 3) at least one of the measured signals is, in part, due to other sources. If $\gamma(f)=1$, the two signals are clearly defined and linearly related at frequency f. When $\gamma(f)=0$, the signals are completely unrelated. This Note shows that such information can be used to tentatively establish that interaction tones based on sum frequencies are more closely related to circumferential velocity components between the propellers whereas tones at difference frequencies are more closely related to axial flow fluctuations.

Discussion

Experiments were performed with counter-rotating hobby aircraft propellers. The two-bladed propellers had a tip diameter of 0.28 m, the pitch was 0.18 m, and were axially separated by $0.1r_t$, where r_t was the tip radius. The right- and left-hand counter-rotation propellers were powered with small electrical motors at speeds of near 20 rps. A single-sensor hot-film anemometer was placed at an axial location halfway between the propellers at a radial location of $0.5r_t$. The microphone was located $0.6r_t$ in front of the leading edge of the forward propeller and at a radial position of $0.82r_t$. The tests were performed inside an anechoic chamber where the propellers were operated at zero advance ratio, i.e., the propellers were fixed in a static fluid environment. Figures 1 and 2 represent typical results from this configuration; however, 36 sets of data were obtained at various transducer spatial locations and two rotor spacings.

Acoustic tests were also performed in the anechoic chamber without the propellers rotating. It was determined that the background noise associated with the experiment was not negligible at all frequencies but was a minimum of 15 dB below the measured CRP noise for all frequencies of concern. Background noise is comparable to test data at frequencies below 20 Hz. Tones that occurred in the background noise level did not correspond in frequency to interaction tones, and coherence between background noise and the background anemometer signal produced significant values only at frequencies that were multiples of 60 Hz.

To determine the microphonic characteristics of the hot-film anemometer, a speaker excited with one-octave-band